Glass–liquid–glass reentrance in mono-component colloidal dispersions

2008 J. Phys.: Condens. Matter 20 205104

(http://iopscience.iop.org/0953-8984/20/20/205104)

J. Phys.: Condens. Matter **20** (2008) 205104 (13pp) doi:10.1088/0953-8984/20/20/205104

Glass–liquid–glass reentrance in mono-component colloidal dispersions

P E Ramírez-González[1], A Vizcarra-Rendón[2], F de J Guevara-Rodríguez[3] and M Medina-Noyola[1]

[1] Instituto de Física 'Manuel Sandoval Vallarta', Universidad Autónoma de San Luis Potosí, Álvaro Obregón 64, 78000 San Luis Potosí, SLP, Mexico
[2] Unidad Académica de Física, Universidad Autónoma de Zacatecas, Paseo la Bufa y Calzada Solidaridad, 98600, Zacatecas, Zac., Mexico
[3] Coordinación de Ingeniería Molecular, Instituto Mexicano del Petróleo, Eje Central Lázaro Cárdenas 152, 07730 México, DF, Mexico

Received 7 January 2008, in final form 13 March 2008
Published 17 April 2008
Online at stacks.iop.org/JPhysCM/20/205104

Abstract

The self-consistent generalized Langevin equation (SCGLE) theory of colloid dynamics is employed to describe the ergodic–non-ergodic transition in model mono-disperse colloidal dispersions whose particles interact through hard-sphere plus short-ranged attractive forces. The ergodic–non-ergodic phase diagram in the temperature–concentration state space is determined for the hard-sphere plus attractive Yukawa model within the mean spherical approximation for the static structure factor by solving a remarkably simple equation for the localization length of the colloidal particles. Finite real values of this property signals non-ergodicity and determines the non-ergodic parameters $f(k)$ and $f_s(k)$. The resulting phase diagram for this system, which involves the existence of reentrant (repulsive and attractive) glass states, is compared with the corresponding prediction of mode coupling theory. Although both theories coincide in the general features of this phase diagram, there are also clear qualitative differences. One of the most relevant is the SCGLE prediction that the ergodic–attractive glass transition does not preempt the gas–liquid phase transition, but always intersects the corresponding spinodal curve on its high-concentration side. We also calculate the ergodic–non-ergodic phase diagram for the sticky hard-sphere model to illustrate the dependence of the predicted SCGLE dynamic phase diagram on the choice of one important constituent element of the SCGLE theory.

(Some figures in this article are in colour only in the electronic version)

1. Introduction

The fundamental understanding of dynamically arrested states is a major challenge of contemporary statistical physics and materials science [1–3]. Model experimental colloidal suspensions, whose static and dynamic properties have been the subject of attention in their own right [4–6], have played an essential role in the study of dynamic arrest phenomena, providing experimental realizations in finely controlled systems and conditions [7, 8]. First-principles models and theories that predict and describe these transitions constitute an essential aspect of the fundamental understanding of these phenomena. The mode coupling theory (MCT) of the ideal glass transition [3, 9] is perhaps the most comprehensive theory of this sort, some of whose predictions have found beautiful experimental confirmation. This is illustrated, for example, by the MCT predictions of the existence and properties of the glass transition in hard-sphere systems [10, 7], and of the existence of a second kind of glass state, referred to as attractive glasses [11–13], that appears when the effects of the short-ranged attractive interactions compete with the effects of hard-sphere forces. The experimental observation of this richer glass transition scenario has been reported in systems in which the attractive interactions originate from some form of solvophobic effect [14–16] or as the result of depletion forces [17–20]. Thus, it is now clear that the effects of attractive forces is to widen the ergodic region in the phase diagram and to introduce a reentrant glass transition at high volume fractions, and low-density arrested states at low volume fractions.

Although there is a remarkable consistency between the predicted MCT general scenario and these experimental observations, the understanding of the detailed nature of these new glass states and the general topology of the ergodic–non-ergodic phase diagram, cannot be considered settled questions. Recent computer simulation work, for example, suggests that the glass transition line intersects the spinodal curve on the high-concentration side, never lying above the critical point [21]. This result could have very important implications in the understanding of the gel-transition mechanism. Similarly, it has recently been suggested [22] that the two-component extension of MCT fails to predict the reentrant behavior that its one-component version does predict, when applied to the conditions for which the glass–liquid–glass reentrance is observed in systems with depletion forces. Questions of this sort seem to be pushing the predictive capability of MCT to its limit, and have prompted the proposal of extended versions of this theory [23–25], or the development of alternative approaches [26]. The main aim of this paper is to apply a recently developed theory of dynamic arrest in colloidal dispersions [27–29] to the description of the glass transition in model systems with attractive interactions. In this paper we report the scenario that emerges when the mono-component version of this theory is applied to a generic system with hard-sphere plus attractive Yukawa interactions, regardless of the physical origin of these attractive forces. One important objective of this work is also to contrast the scenario predicted by the present theory with that predicted by conventional MCT [11].

The theory we refer to is essentially the application of the self-consistent generalized Langevin equation (SCGLE) theory of colloid dynamics [30–33] to the analysis of dynamic arrest phenomena in specific colloidal systems and conditions. The SCGLE theory was originally devised to describe the tracer and collective diffusion properties of colloidal dispersions in the short- and intermediate-time regimes. As explained in [28], its self-consistent character introduces a nonlinear dynamic feedback, leading to the prediction of dynamic arrest in these systems, similar to that exhibited by the mode coupling (MC) theory of the ideal glass transition. The application of this theory was illustrated with the comparison of its predictions regarding the glass transition in two monodisperse experimental systems with specific (hard-sphere and screened electrostatic) inter-particle effective forces [28]. For these systems the SCGLE theory was found to have similar quantitative predictive power as conventional MCT, but with a lower degree of difficulty in its application [29]. Some aspects of the application of the SCGLE theory to systems with short-ranged attractive interactions were briefly reported in a recent short communication [27], and the present paper contains a more systematic discussion on this subject.

We start in the following section by reviewing the basics of the SCGLE theory of dynamic arrest. In section 3 we describe the resulting dynamic arrest phase diagram of the hard-sphere plus attractive Yukawa model. In section 4 we briefly present the main features of the corresponding non-ergodic parameters of the HSAY system. Since these properties derive rather directly from the static structure factors employed as input of the dynamic theory, in section 5 we discuss the main features of these static inputs, provided by the semi-analytic solution of the mean spherical approximation. In section 6 we discuss the possible contact of our theoretical results with the available experimental measurements. In section 7 we present the dynamic arrest phase diagram of a simple toy model, namely, the sticky hard-sphere model, with the intention of comparing the different dynamic arrest scenarios predicted by our theory and by MCT, and with the intention of analyzing the dependence of the SCGLE results on one fundamental element of this theory. Section 8 summarizes the main results and gives the conclusions of this paper.

2. Brief review of the SCGLE theory

The dynamic properties of colloidal dispersions can be described in terms of the relaxation of the fluctuations $\delta n(\mathbf{r}, t)$ of the local concentration $n(\mathbf{r}, t)$ of colloidal particles around the bulk equilibrium value n. The average decay of $\delta n(\mathbf{r}, t)$ is described by the time-dependent correlation function $F(k, t) \equiv \langle \delta n(\mathbf{k}, t)\delta n(-\mathbf{k}, 0)\rangle$ of the Fourier transform $\delta n(\mathbf{k}, t) \equiv (1/N)\sum_{i=1}^{N} \exp[\mathrm{i}\mathbf{k}\cdot\mathbf{r}_i(t)]$ of the fluctuations $\delta n(\mathbf{r}, t)$, with $\mathbf{r}_i(t)$ being the position of particle i at time t. $F(k, t)$ is referred to as the intermediate scattering function, measured by experimental techniques such as dynamic light scattering. One can also define the *self*-component of $F(k, t)$, referred to as the self-intermediate scattering function, as $F_S(k, t) \equiv \langle \exp[\mathrm{i}\mathbf{k}\cdot\Delta\mathbf{R}(t)]\rangle$, where $\Delta\mathbf{R}(t)$ is the displacement of any of the N particles over a time t. The self-consistent generalized Langevin equation theory of colloid dynamics [30–33] leads to the calculation of $F(k, t)$ and $F_S(k, t)$, given the effective interaction pair potential $u(r)$ between colloidal particles and the corresponding equilibrium static structure, represented by the static structure factor $S(k)$.

This theory is based on general and exact expressions for $F(k, t)$ and $F_S(k, t)$ in terms of a hierarchy of memory functions complemented by a number of physically or intuitively motivated approximations [30]. The first and most important of such elements consists of general and exact memory function expressions for $F(k, t)$ and $F_S(k, t)$ [30], which in Laplace space read

$$F(k, z) = \frac{S(k)}{z + \frac{k^2 D_0 S^{-1}(k)}{1+C(k,z)}}, \tag{1}$$

$$F_S(k, z) = \frac{1}{z + \frac{k^2 D_0}{1+C_S(k,z)}}, \tag{2}$$

where D_0 is the free-diffusion coefficient, $S(k)$ is the static structure factor of the system, and $C(k, z)$ and $C_S(k, z)$ are the Laplace transform (LT) of the so-called irreducible memory functions $C(k, t)$ and $C_S(k, t)$ [34][4]. These exact results can be derived in a variety of manners, and our derivation [30] was framed within the generalized Langevin equation (GLE) formalism and the process of contraction of the description [36, 37].

[4] In reality, Nägele *et al* [34] refer to $[C(k, z)D_0]$ as the 'irreducible memory function', a concept first introduced by Cichocki and Hess [35].

The second ingredient of the SCGLE theory is the intuitive notion that collective and self-dynamics may be connected in a simple manner. Vineyard's approximation [38], in which the collective propagator $\Psi(k,t) \equiv F(k,t)/S(k)$ is approximated by the 'self'-propagator $\Psi^{(s)}(k,t) \equiv F^{(s)}(k,t)$, is the most primitive (or 'zeroth order') implementation of this idea. Equations (1) and (2) suggest, however, that other connections between self-and collective dynamics may be proposed at the level of the memory functions $C(k,z)$ and $C_{\rm S}(k,z)$, the simplest of them being to approximate one by the other, namely,

$$C(k,t) = C_S(k,t). \tag{3}$$

This is referred to as the first-order Vineyard approximation, and is the approximation that we shall incorporate in the SCGLE theory of dynamic arrest introduced in the present work. In spite of its apparent simplicity (or, in fact, because of its simplicity), this turns out to be the formal connection between collective and self-dynamics that best serves the purpose of describing the long-time slow dynamics of systems near their dynamic arrest transitions. It is the best not only because it is the simplest, but also because it turns out to be equally accurate, for the purposes given above, as other more sophisticated higher-order Vineyard approximations. For example, given that the SCGLE theory was originally aimed at describing short- and intermediate-time properties, the difference $[C(k,t) - C_{\rm S}(k,t)]$ was approximated by the difference of the exact short-time/large-k limit $C^{\rm SEXP}(k,t)$ and $C_{\rm S}^{\rm SEXP}(k,t)$ of these memory functions, for which well-established expressions are available in terms of equilibrium structural properties [6, 39, 28]. As was discussed more recently [29], however, an equally accurate approximation is to simply neglect this difference, and to relate the two irreducible memory functions by the simpler relation in equation (3).

The third ingredient consists of the independent approximate determination of $F_{\rm S}(k,t)$ [or $C_{\rm S}(k,t)$]. One intuitively expects that these k-dependent self-diffusion properties should be simply related to the properties that describe the Brownian motion of individual particles, just like in the Gaussian approximation [4], which expresses $F_{\rm S}(k,t)$ in terms of the mean-squared displacement $W(t)$ as $F_{\rm S}(k,t) = \exp[-k^2 W(t)]$. We introduce an analogous approximate connection, but at the level of their respective memory functions. The memory function of $W(t)$ is the so-called time-dependent friction function $\Delta\zeta(t)$. This function, normalized by the solvent friction $\zeta_0 = (\beta D_0)^{-1}$, is the long wavelength limit of $C_{\rm S}(k,t)$, i.e. $\lim_{k\to 0} C_{\rm S}(k,t) = \Delta\zeta^*(t) \equiv \Delta\zeta(t)/\zeta_0$. Thus, we interpolate $C_{\rm S}(k,t)$ between its two exact limits, $C_{\rm S}(k,t) = C_{\rm S}^{\rm SEXP}(k,t) + [\Delta\zeta^*(t) - C_{\rm S}^{\rm SEXP}(k,t)]\lambda(k)$, with $\lambda(k)$ being a phenomenological interpolating function such that $\lambda(k \to 0) = 1$ and $\lambda(k \to \infty) = 0$. In the absence of rigorous fundamental guidelines to construct this interpolating function, we require $\lambda(k)$ to represent the optimum mixing of these two limits of $C_{\rm S}(k,t)$ in the simplest possible analytical manner. Guided by these practical considerations, in [30] the proposal was made to model $\lambda(k)$ by the functional form $\lambda(k) \equiv [1 + (k/k_{\rm c})^{\nu}]^{-1}$, in which the parameter ν indicates how abruptly the memory function $C_{\rm S}(k,t)$ crosses over from its small-k to its large-k value, and the parameter $k_{\rm c}$ indicates at which wavevector this crossover will occur.

The parameters ν and $k_{\rm c}$ could, of course, be treated simply as adjustable parameters, determined every time by the comparison with specific experimental or simulated data. This, however, is not what the SCGLE theory advocates. The proposal in [30] involved, instead, a less empirical strategy, based on the expectation that these parameters could be determined in a more general and universal manner, independent of the details of the specific system. Hopefully, such a universal protocol could be revealed by its application to an arbitrary (experimental or simulated) system. With this expectation in mind, in [30] theoretical predictions of the collective dynamics of a specific system (a two-dimensional repulsive Yukawa Brownian fluid) were calculated using a variety of values of ν and $k_{\rm c}$. These results were then compared with ('exact') Brownian dynamics simulations for $F(k,t)$ for a fixed state. In this manner it was discovered that the optimum choice of these parameters was $\nu = 2$ and $k_{\rm c} = k_{\rm min}$, with $k_{\rm min}$ being the position of the first minimum that follows the main peak of the static structure factor $S(k)$. The expectation is, of course, that this choice is equally useful under more general conditions, including, of course, other states of the same system and other (simulated or experimental) systems. In [31] this expectation was reasonably confirmed for simulated mono-disperse systems, and in [33] for model colloidal mixtures. The same definition of these parameters was also successfully employed in the comparison in [28] of the predictions of the present theory with the experimental data for the non-ergodicity parameters in dispersions of highly charged particles and of hard-sphere particles at high concentrations (the latter involving strong hydrodynamic interactions). Although one could imagine possible refinements to this protocol, in this work we maintain this definition of $\lambda(k)$. Furthermore, we adopt a simplified version of the interpolation formula above, due to the fact that the present work deals with the long-time slow relaxation processes near the dynamic arrest transition, for which the short-time details described by the short-time memory function $C_{\rm S}^{\rm SEXP}(k,t)$ are not expected to be relevant. Thus, the interpolating formula above simplifies to

$$C_{\rm S}(k,t) = \left[\Delta\zeta^*(t)\right]\lambda(k), \tag{4}$$

which we incorporate in the present self-consistent theory.

The fourth ingredient of our theory is another exact result, this time for $\Delta\zeta^*(t)$. In [36] the effective Langevin equation of a tracer colloidal particle interacting with the other particles of a mono-disperse suspension was derived, using the concept of contraction of the description [37] (a summary of such derivation is contained in appendix B of [28]). Besides the solvent friction force, $-\zeta^0\mathbf{V}(t)$, the direct interactions of the tracer particle with the other particles give rise to an additional friction term of the form $-\int_0^t {\rm d}t' \Delta\zeta(t-t')\mathbf{V}(t')$, where $\mathbf{V}(t)$ is the tracer particle's velocity at time t. In the process, an exact result for the time-dependent friction function $\Delta\zeta^*(t) \equiv \Delta\zeta(t)/\zeta^0$ is generated. This exact result may, upon the introduction of two well-defined simplifying approximation (referred to as the 'homogeneous fluid' and

the 'decoupling' approximations [36]), be converted into the following approximate but general expression

$$\Delta\zeta^*(t) = \frac{D_0}{3\,(2\pi)^3\,n}\int \mathrm{d}\mathbf{k}\left[\frac{k[S(k)-1]}{S(k)}\right]^2 F(k,t)F_S(k,t). \tag{5}$$

The incorporation of this result finally leads to a closed system of equations.

Thus, equations (1)–(5) constitute the SCGLE theory of colloid dynamics. Besides the unknown dynamic properties, it only involves the static structural property $S(k)$, determined by the methods of equilibrium statistical thermodynamics, and the interpolating function $\lambda(k)$, which also depends on $S(k)$. Notice that the resulting self-consistent scheme is free from any form of adjustable parameters. Let us also mention that equations (1) and (2) are exact results, and equation (5) derives from another exact result. Hence, it should not be a surprise that the same results are employed by other theories; in fact, the same equations are employed in MCT. The difference lies, of course, in the way we relate them and use them. In this sense, the distinctive elements of our theory are the Vineyard-like approximation in equation (3) and the interpolating approximation in equation (4).

From the SCGLE scheme in equations (1)–(5) one can derive the equations for its long-time asymptotic solutions. Thus, the unknown dynamic properties $F(k,t)$, $F_S(k,t)$, $C(k,t)$, $C_S(k,t)$, and $\Delta\zeta^*(t)$, which in an ergodic state decay to zero, in a non-ergodic state decay to finite asymptotic values, referred to as the non-ergodic parameters, which we denote by $f(k)S(k)$, $f_S(k)$, $c(k)$, $c_S(k)$, and $\Delta\zeta^{*(\infty)}$. One can then re-write equations (1)–(5) in terms of these asymptotic values plus a regular contribution that does decay to zero. Taking the long-time limit of the resulting equations leads to a system of five equations for these five unknown non-ergodic parameters [28, 29]. This system of equations can easily be reduced to a single equation for the scalar parameter $\Delta\zeta^{*(\infty)}$, which reads

$$\frac{1}{\gamma} = \frac{1}{6\pi^2 n}\int_0^\infty \mathrm{d}k\, k^4 \frac{[S(k)-1]^2\,\lambda^2(k)}{\left[\lambda(k)S(k)+k^2\gamma\right]\left[\lambda(k)+k^2\gamma\right]}, \tag{6}$$

with γ defined as $\gamma \equiv D_0/\Delta\zeta^{*(\infty)}$. The parameter γ thus defined is just the asymptotic long-time value of the mean-squared displacement of a particle localized by the arrested cage formed by its neighbors [28]. The very form of this criterion exhibits its simplicity: given the effective inter-particle forces, statistical thermodynamic methods allow us to determine $S(k)$, and the absence or existence of *finite* positive real solutions of this equation will indicate if the system remains in the ergodic phase or not (notice that $\gamma = \infty$ is always a solution, representing ergodic states). The meaning of $\sqrt{\gamma}$ as the localization length of a tracer particle in the glass follows from the fact that the effective force on such a tracer particle includes a term given by [36] $\zeta_0\int_0^\infty \Delta\zeta^*(t-t')\mathbf{v}(t')\,\mathrm{d}t'$; in an arrested state, the non-ergodic part of $\Delta\zeta^*(t)$ generates a harmonic force whose elastic constant, given by $\zeta_0\Delta\zeta^{*(\infty)}$, is related to γ by the definition above, through the equipartition theorem.

The other four equations for the non-ergodic parameters can then be used to express those quantities in terms of γ. The equations for the non-ergodic parameters $f(k)$ and $f_S(k)$ then read

$$f(k) = \frac{\lambda(k)S(k)}{\lambda(k)S(k)+k^2\gamma} \tag{7}$$

and

$$f_S(k) = \frac{\lambda(k)}{\lambda(k)+k^2\gamma}. \tag{8}$$

These equations clearly show that γ and the non-ergodic parameters $f(k)$ and $f_S(k)$ only depend on the static structure factor $S(k)$ (and the interpolating function $\lambda(k)$, which is determined by $S(k)$), and not on transport properties, such as D_0.

3. Hard-sphere plus attractive Yukawa model

Let us now discuss the application of the SCGLE theory above, to the description of dynamic arrest in colloidal systems with hard-sphere plus short-ranged attractive interactions. Strictly speaking, the mono-component version of the SCGLE theory should provide an appropriate description of the dynamic arrest phenomena in these systems only when no second colloidal or macromolecular component is involved. Thus, we shall have in mind mono-disperse colloidal dispersions with attractive interactions that originate, for example, from some form of solvophobic effects. Since depletion forces are induced by a second colloidal species, whose dynamics is not explicitly included in the present model, their description should in principle lie outside the present discussion. The application of the SCGLE theory requires the static structure factor $S(k)$ to be provided as an external input. This structural property may either be determined experimentally, by computer simulations, or by approximate statistical thermodynamic theories. The latter approach starts with the definition of the inter-particle pair potential $u(r)$ leading, with the assistance of specific liquid theory approximations [40], to an approximate evaluation of $S(k)$.

In this section we present the results of the application of the SCGLE theory to the hard-sphere plus attractive Yukawa (HSAY, or simply 'attractive Yukawa') system, defined by the pair potential

$$\beta u(r) = \begin{cases} \infty, & r < \sigma; \\ -K\dfrac{\exp[-z(r/\sigma-1)]}{(r/\sigma)}, & r > \sigma. \end{cases} \tag{9}$$

Since at this stage we are interested mostly on the qualitative predictions of our theory, and in highlighting the main differences and similarities with the predictions of MCT, here we shall adopt the mean spherical approximation (MSA) for the calculation of the static structure factor of this model, taking advantage of its semi-analytic solution [41]. The state space of this system is spanned by the hard-sphere volume fraction $\phi \equiv \pi n\sigma^3/6$ and by the dimensionless parameters z and K, representing the inverse decay length (in units of the hard-sphere diameter σ) and the depth (in units of k_BT) of the attractive Yukawa well. For fixed z, the equilibrium

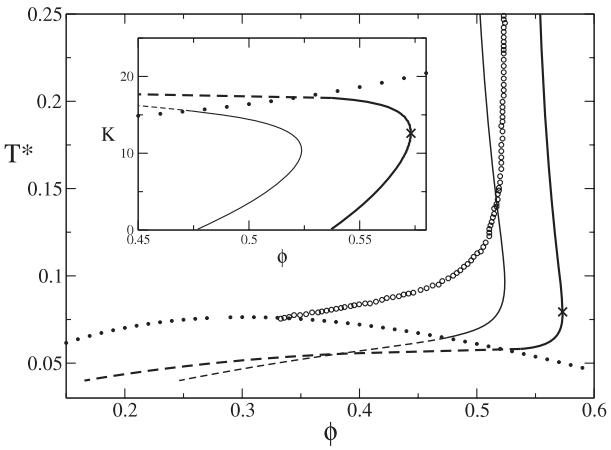

Figure 1. Theoretical glass transition line in the plane (T^*, ϕ) for the HSAY system with fixed $z = 20$ according to the SCGLE theory, calculated with equation (6), and represented by the thick (solid and dashed) curve. The lighter (solid and dashed) line corresponds to the freezing line, according to the Hansen–Verlet criterion, and the dotted curve corresponds to the spinodal line. For reference, we also include the glass transition line predicted by MCT (symbols taken from [11]). The inset re-plots the SCGLE glass transition, the freezing, and the spinodal lines in the (ϕ, K) plane. The symbol '×' indicates the high-concentration end point $(\phi_e, T_e^*) = (0.574, 0.0794)$ of the glass transition line.

phase diagram of this system in the state space (ϕ, T^*), with $T^* \equiv K^{-1}$ being a reduced temperature contains the gas, liquid, and solid phases. The gas–liquid transition involves a coexistence region, with an associated spinodal line $\phi = \phi_s(T^*)$. The liquid–solid transition also involves a coexistence region limited by the freezing and the melting lines $\phi = \phi_f(T^*)$ and $\phi = \phi_m(T^*)$. The spinodal and the freezing lines are readily sketched from the static structure factor by the respective conditions, namely, $S^{-1}(k = 0) = 0$ and $S(k = k_{max}) = 2.85$ (Hansen–Verlet criterion [42], with k_{max} being the position of the main peak of $S(k)$). In figure 1 we present the spinodal and the freezing lines thus determined for the HSAY system with $z = 20$ using the static structure factor provided by the MSA.

These elements of the equilibrium phase diagram serve as a reference in plotting the SCGLE results for the ergodic–non-ergodic transition line calculated with the procedure of the previous section, also employing the MSA static structure factor as static input. In order to compare these results with those of MCT, we have also included the MCT transition line calculated in [11] with the same static input. Let us first notice that, as the temperature is decreased starting from the hard-sphere limit, our results for the glass transition line $\phi = \phi_g(T^*)$ move to slightly higher volume fractions until $\phi_g(T^*)$ reaches a maximum value ϕ_e at the high-concentration end point (ϕ_e, T_e^*). Upon decreasing the temperature below T_e^*, the transition line moves very rapidly to lower volume fractions until meeting the spinodal line on its high-density side. Let us notice that the freezing line follows a similar trajectory, i.e. it first moves to the right, up to its own end point, and then moves to the left until meeting the spinodal line. In fact, the freezing and the glass transition lines follow rather parallel trajectories, since they keep the separation $[\phi_g(T^*) - \phi_f(T^*)]$ roughly temperature-independent in the region outside the spinodal. The dashed lines inside the spinodal are the extrapolation of the glass and freezing transitions to the inside of the spinodal, using the analytic continuation of the MSA static structure factors; we mention that the small-k divergence of $S(k)$ at the spinodal does not strongly affect the evaluation of the integral in equation (6), and that the analytic continuation of $S(k)$ for wavevectors near its main peak (which determine the glass and freezing transition lines) evolves smoothly from the outside to the inside of the spinodal. Although we still have to discuss in more detail the physical meaning of the results inside the spinodal, we report that the SCGLE glass and freezing transition lines only intersect inside the spinodal. We found this to be a general pattern for the other values of the parameter z considered here (up to $z = 100$).

In contrast, the MCT glass transition line, which for $z = 20$ meets the spinodal line near its critical point, may not cross the spinodal curve for larger values of z. In this regard, recent simulation work [21] reports no sign of the glass transition line to preempt the gas–liquid spinodal curve, in agreement with the results of the SCGLE theory. Let us also notice that, in contrast with the predictions of the SCGLE theory, the MCT glass transition line crosses the (Hansen–Verlet) freezing line at temperatures well above the spinodal curve. We must mention, however, that in recent calculations of the freezing and (MCT) glass transition lines, computed with more accurate static structure factors and for $z = 30$, no crossing between these two lines is reported, although a decrease of $[\phi_g(T^*) - \phi_f(T^*)]$ with temperature down to $T^* \approx 1$ is observed; see figure 1 of [43].

The inset of figure 1 re-plots the SCGLE glass transition line at its high-density end, now in the plane (K, ϕ), to illustrate the SCGLE prediction of the reentrant behavior of the system upon lowering its temperature (raising K) at fixed volume fraction. This reentrance was first qualitatively predicted by MCT [11–13] and some of its features have been observed in specific experimental systems [14–20]. The detailed quantitative comparison between experimental measurements and theoretical predictions is still a matter of investigation.

Let us now illustrate the dependence of the location of the glass transition line on the parameter z representing the inverse range of the attractive forces. This is done in figure 2(a), where we observe that the trends regarding the location of the end point are rather similar to those obtained by Bergenholtz and Fuchs from mode coupling theory [11], i.e. the end point moves to higher volume fractions and lower reduced temperatures with increasing z. As already indicated, the transition line of the SCGLE theory intersects the spinodal on the high-concentration side of the latter. In the inset of this figure we use dashed lines to denote the analytic continuation of the transition line inside the spinodal. Notice also that at large temperatures (say, $T^* \gtrsim 1$), the dependence on z of the glass transition line vanishes, at least for z in the range considered here.

From the theoretical results illustrated in figure 2(a) we may extract the z-dependence of ϕ_e, the volume fraction of the high-concentration end point of the glass transition line.

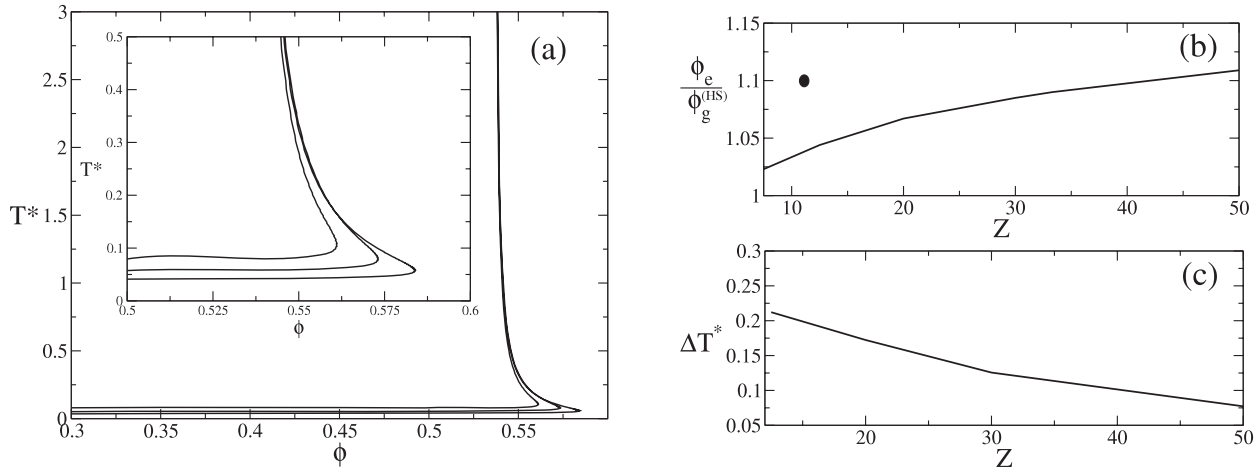

Figure 2. (a) Theoretical glass transition line in the plane (ϕ, T^*) for the HSAY system for $z = 12.5$, 20, and 30. (b) Volume fraction ϕ_e of the high-concentration end point of the glass transition line (in units of the hard-sphere glass transition volume fraction $\phi_g^{(HS)}$), as a function of z; the solid circle corresponds to the conditions of the experimental system in [18]. (c) Width ΔT^* of the reentrance ergodic region (defined in the text) as a function of z.

This property, expressed in units of the hard-spheres glass transition volume fraction $\phi_g^{(HS)}$, is plotted in figure 2(b), which shows that ϕ_e increases monotonically with z. One may assume that scaled properties such as the ratio $\phi_e/\phi_g^{(HS)}$ depend less strongly on the numerical inaccuracies of the specific theoretical models or approximations (such as the actual value of the hard-sphere glass transition volume fraction) or on the assumed connection between the experimental control parameters and the theoretical state parameters (K, z, and ϕ). Thus, this information may be relevant in attempting a direct connection between the results of the SCGLE theory with the few experiments in which not only the reentrance phenomenon has been confirmed but also the glass transition line has been sketched and the position of the end point has been estimated.

We can observe in figure 2 that, as z increases, not only the end point moves to the right but also the shape of the ergodic protrusion ending at (ϕ_e, T_e^*), i.e. of the reentrance region, becomes more pronounced and acute. One might then question if, in the limit $z \to \infty$, this protrusion might become thin enough to mimic the glass–glass transition line predicted by MCT for the hard-sphere plus square well model in the regime of deep and thin wells [13]. The answer is that, although the observed tendency is the thinning of this protrusion with increasing z, such limiting behavior is not reached, at least for the values of z considered here ($z \leqslant 100$). To illustrate this, in figure 2(c) we show how the width ΔT^* of this protrusion changes with increasing z. We define ΔT^* as the temperature difference between the points at which the glass transition line is intersected by the isochore $\phi = [\phi_e - \phi_g^{(HS)}]/2$ (which lies midway between the isochores $\phi = \phi_g^{(HS)}$ and $\phi = \phi_e$ that limit the reentrance region).

4. Non-ergodic parameters

The non-ergodic parameter $f(k)$ can be easily calculated using equation (7). Illustrative examples are given in figure 3, where we plot two sequences exhibiting the evolution of the k-dependence of $f(k)$ as we lower the temperature (or increase the coupling parameter K). In figure 3(a) we decrease the temperature along the glass transition line for $z = 30$ from hard-sphere-like conditions ($K = 0.1$), through the repulsive glass regime, passing the end point (ϕ_e, T_e^*) and the attractive glass region down to near the spinodal line. We observe a monotonic increase of $f(k)$ at most wavevectors as temperature is lowered, a trend similar to that observed by Bergenholtz and Fuchs [11] in the results of MCT. We notice, however, that the changes in the height of $f(k)$ in the vicinity of the position k_{max} of the main peak of $S(k)$ are much smaller than at other wavevectors. Also notice that the position of the maximum of $f(k)$ shifts to slightly larger values of k as we pass the end point (ϕ_e, T_e^*), from repulsive to attractive glasses. In the inset of figure 3(a) we plot the corresponding *self*-non-ergodic parameter $f_s(k)$. We notice that this property exhibits a less dramatic evolution as the temperature is lowered. In fact, the self-non-ergodic parameters corresponding to the largest values of K ($K = 20$ and 25) are virtually indistinguishable on the scale of the figure.

The sequence in figure 3(b) corresponds to an isochoric process of the HSAY system with $z = 20$. The fixed volume fraction of this isochore, $\phi = 0.558$, is intermediate between $\phi_g^{(HS)} = 0.537$ and $\phi_e = 0.574$, and hence it crosses the reentrance region. Here we observe a non-monotonic evolution of $f(k)$ as temperature is lowered (K is increased). Thus, in a first stage, starting from the hard-sphere regime towards the repulsive glass transition, $f(k)$ decreases at most wavevectors as temperature is lowered, whereas for temperatures below the attractive glass transition, $f(k)$ increases as we further lower the temperature. The results in figure 3 clearly exhibit a general feature of the predictions of the SCGLE theory for the *collective* non-ergodic parameter $f(k)$, namely the fact that its small-k limit is always 1. This limit is built in the theory and is introduced by the approximations involved. We notice that MCT predicts, instead, that $\lim_{k\to 0} f(k) < 1$. Besides this rather notorious discrepancy, the SCGLE theory and MCT

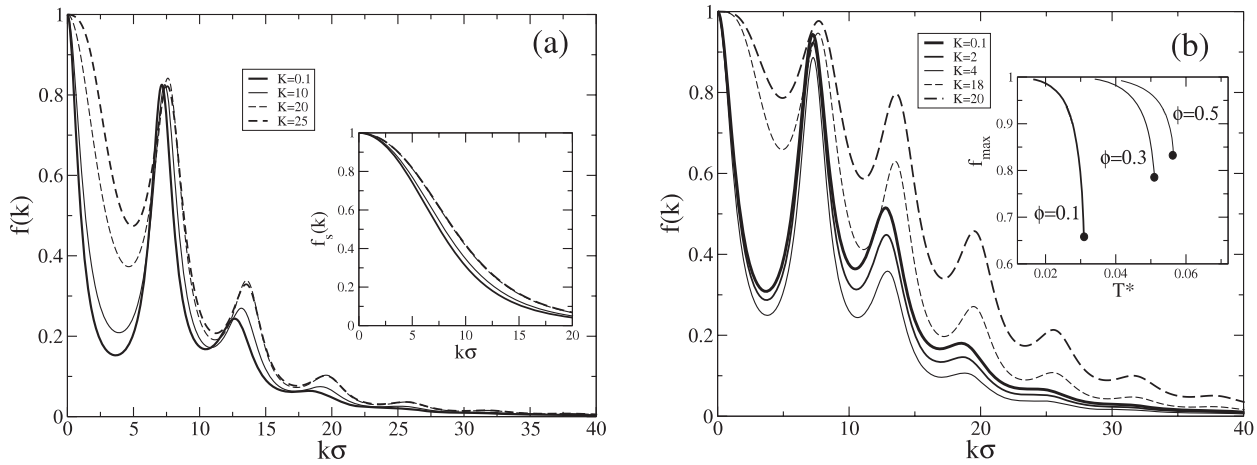

Figure 3. Non-ergodic parameter $f(k)$ as a function of wavevector of the HSAY model with fixed z, calculated from equation (7) using MSA static structure factors. In (a) we have fixed $z = 30$ and varied ϕ and K to follow the glass transition line. The inset shows the corresponding self-non-ergodic parameter. In (b) we have fixed $z = 20$ and $\phi = 0.558$, and varied K. The inset contains the variation of the maximum $f_{\max}$ of $f(k)$ as a function of T^* as we decrease T^* from its value at the transition line (circles) along the isochores $\phi = 0.1,\ 0.3$, and 0.5, for $z = 20$.

seem to agree on the main qualitative features of $f(k)$ that we just described.

The changes in $f(k)$ illustrated in figure 3 occur in a limited window of volume fractions and reduced temperatures. We have scanned the state space to see the evolution of the non-ergodic parameter, and in the inset of figure 3(b) we illustrate the results of this scanning, in terms of the maximum value $f_{\max}$ of the non-ergodic parameter as a function of T^* along the isochores $\phi = 0.1$, 0.3, and 0.5 (for $z = 20$). The general pattern for all these isochores, and for the other values of z considered here, is that $f_{\max}$ increases as temperature is lowered below its glass transition temperature $T_g^*(\phi)$, and that $f_{\max}$ tends to saturate at the value $f_{\max} \approx 1$ at low enough temperatures. Let us also notice from the results in this inset, that the value of $f_{\max}$ *at* the transition (represented by the solid circles) increases with increasing volume fraction in a much more pronounced manner than illustrated in figure 3(a). One reason is that the volume fraction range covered in the inset is definitely larger than the volume fraction range involved in figure 3(a).

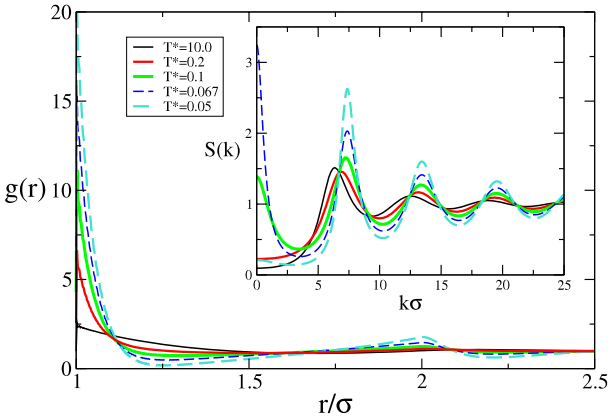

Figure 4. Radial distribution function (main figure) and static structure factor (inset) of the HSAY model with $z = 20$, calculated with the mean spherical approximation at fixed volume fraction $\phi = 0.3$ at various reduced temperatures.

5. Short-range structure and cluster formation

The dynamic arrest scenario emerging from the application of either MCT or the SCGLE theory is the result of two factors, namely, the general approximations and exact results involved in the construction of these dynamic theories, and the detailed static structural information of the specific system studied, employed as an input in a particular concrete application. This structural information, encrypted somehow in the static structure factor $S(k)$, triggers the onset of slow dynamic behavior and the abrupt or discontinuous dependence of the dynamic properties and leads to the reentrant dynamic arrest scenario just described. Nevertheless, $S(k)$ is found to vary quite smoothly and continuously everywhere. Thus, the discontinuity of the dynamic properties implies the existence of dynamic order parameters, such as the long-time self-diffusion coefficient, which depend on $S(k)$ in a continuous manner, but which may reach a threshold value with a relevant dynamic significance, such as $D_L = 0$. In the process, no dramatic change is observed in $S(k)$, whose main features vary monotonically as the transition line is crossed. For this very reason, it is important to scrutinize $S(k)$ and $g(r)$ in an attempt to identify which features of these structural properties might be responsible for driving the system to the dynamic arrest scenario described above.

Thus, we start in figure 4 by plotting the evolution of $g(r)$ and $S(k)$ as we lower the temperature at fixed $\phi = 0.3$ for the HSAY system with $z = 20$. The first important observation refers to the effects of the long-ranged correlations associated to the critical point and, in general, to the spinodal line. These effects are clearly noticed in the large values of $S(k = 0)$ near the spinodal (see the inset of figure 4). They also influence

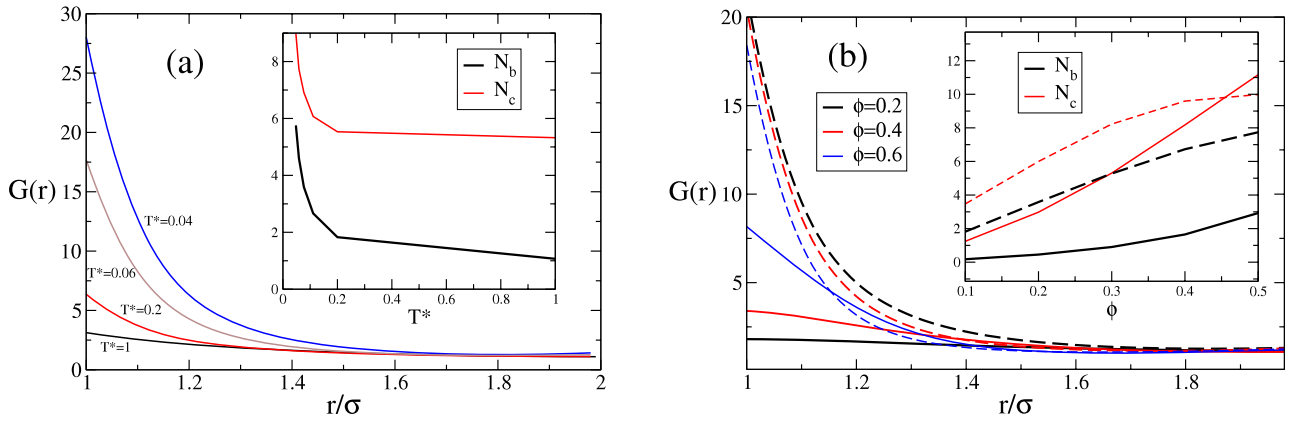

Figure 5. Local compactness function $G(r)$ (main figures), mean number of bonded particles N_b (thick black lines in the insets), and mean coordination number N_c (thinner (red) lines in the insets) for the HSAY model with $z = 20$. In (a) we have fixed the volume fraction at $\phi = 0.3$ and varied the temperature. In (b) we fixed the temperature at the values $T^* = 1$ ('high' temperature, hard-sphere-like; solid lines; the upper curve corresponds to the largest volume fraction) and $T^* = 0.05$ (low temperature; dashed curves; the upper curve corresponds to the *smallest* volume fraction).

the long-ranged behavior of $g(r)$. This influence, however, is virtually absent in the short-ranged structure of this property, as illustrated in the main figure. In fact, it is quite remarkable that, in spite of their singular nature, these long-ranged correlations at the spinodal line do not seem to have a very relevant effect on the dynamic properties near the dynamic arrest transition. In fact, these dynamic properties can also be evaluated *inside* the spinodal curve employing the analytic continuation of the MSA structure factor illustrated in the figure, and the result is a continuous and monotonous behavior as the spinodal line is traversed. This was already illustrated in figure 1 with the glass transition line, and figure 4 illustrates the same feature in terms of the radial distribution function itself.

In the same figure, however, we can also observe a very apparent monotonic tendency of the particles, in the close neighborhood of a central particle, to arrange themselves in increasingly more compact structures as temperature is lowered. This is evidenced, for example, by the increase in the contact value $g(\sigma+)$. We find that this monotonic trend in the short-ranged structure of $g(r)$ is not affected by the presence of the glass transition or the spinodal curve; instead, this trend is perhaps the origin of the existence of both of these boundaries. Thus, it is important to describe the evolution of the degree of compactness of the local structure as we lower the temperature and/or increase the volume fraction, since this may be an important structural feature associated with the dynamic arrest of the system. Furthermore, the concept of compactness is perhaps a central property of the cluster structures expected to appear when the short-ranged attractions dominate, particularly at low volume fractions. Thus, let us introduce, following [44], the mean number N_b of particles bonded to a central particle and the mean coordination number N_c, which we define as

$$N_b = \int_\sigma^{\sigma+z^{-1}} ng(r)\,\mathrm{d}^3r \tag{10}$$

and

$$N_c = \int_\sigma^{\sigma+r^*} ng(r)\,\mathrm{d}^3r, \tag{11}$$

with r^* being the location of the first minimum of $g(r)$ (in practice, for $z = 20$, we took $r^* \approx 1.3$). More generally, we may extend the definitions above to an arbitrary upper limit r, and normalize the resulting particle number by the mean number of particles in a volume of the same size but in the bulk. Thus, let us define the local compactness of the arrangement of neighboring particles around a given central particle as the function

$$G(r) \equiv \frac{\int_\sigma^r g(r)\,\mathrm{d}^3r}{\int_\sigma^r \mathrm{d}^3r}. \tag{12}$$

In figure 5 we present the evolution of these properties as the state parameters (ϕ, T^*) are varied. In the insets of this figure we also plot the corresponding evolution of the numbers N_b and N_c. The very first feature to notice is that the compactness function, $G(r)$, varies much more dramatically with temperature at fixed volume fraction (particularly when T^* falls below 0.2) than with volume fraction at fixed temperature. This can be observed in figure 5(a) as the large increase of $G(r)$ as we lower T^*; notice, for example, that $G(\sigma+)$ increases from around 3 to near 30 when T^* is decreased from 1 to 0.04. Instead, $G(\sigma+)$ increases from around 2 to 8 when ϕ varies from 0.2 to 0.6 at $T^* = 1$ (see figure 5(b)), and that the curves for $G(r)$ at the lower temperature $T^* = 0.05$ do not differ much for the various volume fractions illustrated in this figure. Another way in which to see this is to compare the evolution of the numbers N_b and N_c in the insets: these numbers increase with volume fraction simply because they are proportional to ϕ, whereas when lowering the temperature at fixed ϕ their increase indicates a clear process of compaction of the short-ranged structure. This conclusion is also supported by the fact that the fraction of particles in the coordination shell that are also bonded, N_c/N_b, is clearly larger at lower temperatures. Notice, however, that these low-temperature features emerge rather dramatically as T^* decreases to values of the order 0.1, which is also the order of magnitude of the critical temperature ($T^* = 0.076$) and of the temperature of the high-concentration end point of the glass transition line ($T^* = 0.079$).

Another important feature to notice is the opposite trend observed at high versus low temperatures in the evolution of $G(r)$ as the volume fraction is varied at fixed temperature. Thus, as observed in the results for this function in figure 5(b), the compactness function increases with the volume fraction along the high-temperature isotherm, whereas the opposite occurs along the low-temperature isotherm. This means that at high temperatures the local structure becomes more compact as the volume fraction increases. This is a natural consequence of the increasing crowding of particles in a fixed volume. Such a 'natural' trend, however, is reversed at low enough temperatures. At low temperatures the strong attractions imply a strong tendency to bonding. The solution to this energy-driven requirement depends, of course, on the availability of particles to bond with, and this depends on volume fraction. Thus, at low volume fractions the only solution is the formation of disconnected clusters, whose compactness is only limited by steric hard-core restrictions. At larger volume fractions, however, these clusters can percolate, and a percolating cluster must balance the energetically driven tendency to bonding, which favors compactness, with the percolation condition, which demands less compact structures. This might explain the opposite trends at high and low temperatures. Of course, a more detailed analysis of these qualitative and quantitative trends of the static structural properties is in order. This first account, provided by the analytic solution of the mean spherical approximation, only allows us to point out that the input structural properties themselves already carry important information, which the dynamic theory expresses in terms of the dynamic arrest scenario that we have described above.

6. Connection with experimental measurements

One of the main difficulties in comparing the results of the present theory of dynamic arrest with specific experimental measurements is the availability of an accurate connection between experimental control parameters and theoretical state variables such as K, z, and ϕ. The accuracy of this connection affects the quality of the comparison between the experimental and the theoretical (equilibrium and dynamic) phase diagrams. We have shown already that in systems where this connection is simple and accurate, and for which the static structure factor has been determined or can be calculated with sufficient accuracy (dispersions of hard or charged spherical particles), the SCGLE theory provides a pretty satisfactory description of dynamic arrest properties such as the non-ergodic parameters [27, 28]. Unfortunately, this is not the situation for systems with short-ranged attractive interactions, since in this case this connection does not seem to be similarly straightforward. For example, in [15], some points of the ergodic–non-ergodic phase diagram were characterized in the space of real control parameters of a copolymer micellar system with short-ranged attractive interactions induced by hydrophobic effects. These points were then mapped onto the state space of the hard-sphere plus square well (HSSW) potential, and MCT was employed to interpret the dynamic measurements. Of course, the topology and other features of the resulting ergodic–non-ergodic phase diagram were determined to a large extent by those of the model and theory employed to establish this mapping. The question remains as to whether the results would be the same if the same raw data were analyzed with a mapping involving instead the attractive Yukawa potential. The fact that the topology of the ergodic–non-ergodic phase diagrams of the two model systems are qualitatively different indicates that the answer is no. MCT predicts that the high-concentration end point of the squared well model is also the end point of a glass–glass transition line, whereas no such glass–glass transition line is predicted by MCT for the attractive Yukawa system [11]; in fact, as indicated in figure 1, the SCGLE theory qualitatively coincides with MCT, concerning this particular feature of the topology of the glass transition line of the attractive Yukawa system.

Thus, since even the very topology of the phase diagram might be under discussion, perhaps one should first focus on properties for which the connection between experimental control parameters and theoretical variables might be more straightforward. This is why we have emphasized the behavior of the ratio $\phi_e/\phi_g^{(HS)}$ plotted in figure 2(b). The hope is that this ratio, which involves only volume fractions, can be calibrated more reliably than the dimensionless temperature parameter T^*. For example, for the experimental system studied in [15], the authors report that the end point is located at $\phi_e = 0.544$, with the volume fraction calibrated in such a way that their $\phi_g^{(HS)}$, rather than coinciding with the actual experimental value ($\sim$0.57), coincides with the mode coupling prediction $\phi_g^{(HS)} = 0.516$. This leads to a ratio $\phi_e/\phi_g^{(HS)} = 1.054$, which, according to our results in figure 2(b), may be obtained with $z \approx 16$. The inverse decay length z^{-1} can be interpreted as the range of the attractive potential in units of the hard-core diameter σ which, according to the estimate $z \approx 16$, must be $\approx$0.06. This estimate is within the experimental range [15] if one establishes a simple relationship between the state space (ϕ, T^*, z) of the attractive Yukawa model and the state space of the squared well system[5]. Beyond this observation, we must postpone the quantitative comparison of our results with the experimental data of [15] until a more accurate correspondence can be established between the experimental data and the theoretical predictions.

Let us mention that another experimental system has been studied which, in a first approximation, might be describable by the present theory. We refer to the colloid–polymer mixtures studied in [18], in which depletion forces arising from the presence of the non-adsorbing polymer are the source of the short-ranged attractive interactions between the colloidal particles. Here the control parameters are the volume fraction ϕ of the colloid and the concentration c_p of the non-adsorbing polymer. It is an experimental fact that this system exhibits a reentrance scenario upon increasing the polymer concentration. This fact has been interpreted as the experimental realization of the reentrance phenomenon predicted by MCT for the generic models of short-ranged

[5] We may relate the parameter z of the attractive Yukawa potential with the parameter $\epsilon \equiv \Delta/\sigma$ of the squared well potential (Δ being the width of the attractive well) by equating the second virial coefficients of these two model potentials. This leads to an approximate relation $\epsilon^{-1} \approx \alpha(T^*)z$, with $\alpha(\infty) = 1$. Reference [14] quotes a value $\epsilon = 0.03$, which, for $z = 16$, corresponds to this relationship taken at $T^* \approx 0.4$.

attractive interactions. At small polymer concentrations, the depletion interactions are well described by the Asakura–Oosawa (AO) effective interaction [45], which provides the connection between the parameters describing this effective interaction and the experimental control parameters. As a result, one finds that the range of the attractive interactions is set by twice the polymer's radius of gyration R_g and that the polymer concentration c_p determines the depth of the attractive well. These connections allowed Pham *et al* [18] to compare the MCT predictions with the experimental data of the dynamic arrest phase diagram. The conclusion was that, although there is full coincidence in the qualitative reentrant behavior, no quantitative agreement could be achieved, particularly with respect to the location ϕ_e of the end point. We have performed a similar exercise using the results of our SCGLE theory for the HSAY model, with essentially the same conclusions. Perhaps the most notorious feature of this comparison is the fact that the SCGLE theory would underestimate the ratio $\phi_e/\phi_g^{(HS)}$, whose experimental value is approximately 1.11. A good estimate of the parameter z of the HSAY model is given by the ratio of the polymer gyration radius to the radius of the colloidal particles, $z \approx 2R_g/\sigma$, whose experimental value is 12.5 [18]. Thus, the point $(z, \phi_e/\phi_g^{(HS)}) = (12.5, 1.11)$ in figure 2(a) (black circle) represents this experiment. The clear displacement of this point from our theoretical predictions (solid curve) indicates the inability of the SCGLE theory and the HSAY model to quantitatively describe this experiment. We find, according to figure 2(a), that the value $\phi_e/\phi_g^{(HS)} = 1.11$ could only be achieved for values of z more than three times larger than the experimental value $z = 12.5$. The question is then whether this disagreement signals a failure of the SCGLE theory of dynamic arrest (or of MCT, which leads to a similar situation), or to the inadequacy of the model whose static structure was employed by these theories or whether, instead, there is nothing intrinsically wrong with these theories and models, but simply the system with depletion interactions cannot be treated as an effective one-component fluid, in terms of a simple effective pair potential such as the Asakura–Oosawa interaction. Although the results above cannot give an answer to this fundamental question, they provide a strong motivation to consider alternative models and more extended theories. The obvious alternative is to consider the extension of MCT or of the SCGLE theory to multi-component dispersions [22], and to treat the colloid–polymer mixtures as what they actually are, namely, a binary colloidal mixture. Preliminary work in this direction, based on the SCGLE theory, seems to indicate that this is indeed a more productive route to the understanding of the experimental data of [18].

7. Sticky hard-sphere model

In this section we consider the application of the SCGLE theory to the sticky hard-sphere (SHS) model. The purpose of these calculations is twofold: to compare the results of the present theory with those of MCT in the context of another simple model system and to illustrate the sensitivity of the predicted dynamic phase diagram to the specific choice of one important constituent element of the SCGLE theory, namely, the interpolating function $\lambda(k)$.

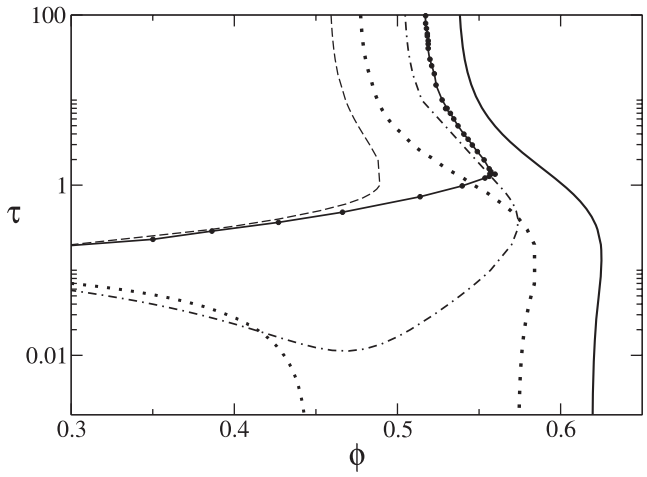

Figure 6. Phase diagram of the sticky hard-sphere (SHS) model in the (ϕ, τ) state space, calculated with the Percus–Yevick static structure factor. The dotted lines are the spinodal curve (lower left) and the Hansen–Verlet freezing line. The other curves correspond to the glass transition line calculated according to the SCGLE theory, equation (6), with $k_c = k_{min}$ (solid curve), with $k_c = \infty$ (dashed curve), and with $k_c = 1.5 \times k_{min}$ (dot–dashed curve). The solid line with black circles is the MCT glass transition line reproduced from [11, 12].

In the sticky hard-sphere model the pairwise forces between particles are described by the hard-sphere potential with diameter σ plus an infinitely deep and narrow well defined as

$$\beta u(r) = \lim_{\delta \to 0} \begin{cases} \infty, & r < \sigma; \\ \ln\left[12\tau\delta/(1+\delta)\right], & \sigma < r < (1+\delta)\sigma; \\ 0, & (1+\delta)\sigma < r, \end{cases} \tag{13}$$

where $\beta^{-1} \equiv k_B T$ is the thermal energy; the parameter τ plays the role of a reduced temperature. The static structure factor of this system is known in closed analytic form within the Percus–Yevick approximation [46] for given τ and given volume fraction $\phi = \pi n \sigma^3/6$ (with n being the particle number concentration). In spite of important limitations, the analytic simplicity of its structural properties makes the SHS system a simple model to practise the application of the SCGLE theory. In figure 6 we present the prediction of the SCGLE theory for the glass transition line in the state space (ϕ, τ). As a reference, we also plot the equilibrium spinodal and the freezing lines (according to the Hansen–Verlet (HV) criterion [42]), as well as the MCT glass transition line reproduced from [11, 12]. In presenting these results, the aim is not so much to draw conclusions about relevant physical content, but to illustrate the level of disagreement between the two theories of dynamic arrest in the context of a simple model system for which fully analytic expressions are available for its static structure factor [46]. Let us first notice that in this case the SCGLE glass transition line never presents the reentrance predicted by the MCT. Instead, it lies completely to the right of the spinodal line, without intersecting it (in reality,

at extremely low τ the glass transition line finally bends to the left, enters inside the spinodal, but immediately gets inside the region where no solution exists for the PY static structure factor). This scenario contrasts completely with that found by Bergenholtz and Fuchs [11] and by Fabbian *et al* [12], who found that the MCT glass transition line is constituted by two different branches that meet at a crossing point, with the low-τ branch continuing beyond this crossing point and ending at a high-concentration end point. As seen in the figure, the low-τ branch does not intersect, but is located above, the spinodal curve. Thus, the SCGLE theory does not predict for this model any form of reentrance nor the presence of a second, low-temperature branch and, hence, neither the glass–glass transition predicted by MCT for this system.

It is interesting to mention, however, that we may distort the results of the SCGLE theory by manipulating one of its essential elements, namely, the interpolating function $\lambda(k) \equiv [1 + (k/k_c)^2]^{-1}$. Thus, using for k_c values different from k_{min}, the position of the first minimum beyond the main peak of $S(k)$, we may distort the results such as the location and shape of the glass transition line. We find that moving k_c to larger k values overemphasizes the effects leading to dynamic arrest. This can be best illustrated by taking the limit $k_c = \infty$, leading to $\lambda(k) = 1$ for all k. The corresponding glass transition line is also plotted in figure 1. Notice that the low-τ part of this distorted glass transition line is located above the spinodal, and, in fact, it behaves rather similarly to the MCT low-τ branch. At large τs, however, it is located completely to the left of the freezing line; in fact, already its hard-sphere limit, $\phi_g^{(HS)}(\tau = \infty) = 0.455$, falls below the corresponding freezing volume fraction. In the same figure we also have plotted another distorted glass transition line, this time corresponding to $k_c = 1.5 \times k_{min}$, only to show that there is a small window of values of k_c around this particular value, where one can see that the transition line does bend to the left, enters the spinodal, and eventually reaches the region inside the spinodal where no solutions for $S(k)$ exist. This distorted transition line happens to mimic more closely the high-τ branch of the MCT glass transition line (in fact, an almost perfect fit of this branch of the MCT glass transition may be achieved with $k_c = 1.2564 \times k_{min}$). In spite of the anomalies of the sticky hard-sphere model, however, these observations serve to illustrate that, at least in the case of the SCGLE theory, the specific choice of the elements that constitute this theory (such as the specific form of $\lambda(k)$) may determine rather crucially the qualitative features of the resulting dynamic arrest scenario.

In addition, the results in figure 6 illustrate the fact that the function $\lambda(k)$ modulates the importance assigned to the large wavevector modes. Thus, the longer ranged this function is in the wavevector domain, the stronger the effects leading to dynamic arrest. The best election of $\lambda(k)$ must, of course, be identified by the highest accuracy of its predictions when compared with clean experimental or simulation data. In this sense, we remind the reader that the definition $k_c = k_{min}$ involved in the SCGLE theory was derived from a series of careful and detailed comparisons with computer simulation results [30, 31], and is considered to be the most reliable choice for this element of the theory. The fact that the SCGLE theory overemphasizes the effects leading to dynamic arrest when taking wavevectors beyond k_{min} suggests that the modes corresponding to the neighborhood of the first maximum of $S(k)$ are the most relevant ones in determining the precise location of the glass transition and that some mechanism should be introduced to suppress the larger-k modes. Such a mechanism is provided in our case by this interpolating function. Of course, one would like elements like this interpolating function to be determined from a rigorous fundamental principle, but this is not the case. Hence, one has to rely on simple and sensible arguments and tests, such as those leading to the definition of $\lambda(k)$ given in the original proposal of the SCGLE theory [30, 31], namely $\lambda(k) \equiv [1 + (k/k_c)^2]^{-1}$, with $k_c = k_{min}$. Most likely one would observe a similar dependence of the results of MCT on the specific definition of the vertex functions, although we are not aware of any systematic discussion of this subject in the literature.

8. Summary

In this paper we have applied the self-consistent generalized Langevin equation theory to the description of dynamic arrest in colloidal dispersions with short-ranged attractive interactions. For this, we adopted the hard-sphere plus attractive Yukawa system of equation (9) as our test model, whose static structure factor $S(k)$ was calculated within the mean spherical approximation. After a brief review of the SCGLE theory, which included the general results for the non-ergodic parameters in equations (6)–(8), the dynamic arrest phase diagram of this model system was presented, its dependence on the range z^{-1} of the attractive forces was illustrated, and the differences and similarities between the results obtained from the SCGLE theory and those obtained from MCT were discussed. Both theories coincide in most qualitative general features, such as the existence of attractive glasses and the reentrance phenomena first described by MCT. Besides obvious quantitative differences, there are also important qualitative disagreements between the predictions of both theories. Perhaps the most notable of them is that the SCGLE theory predicts that the glass transition line always intersects the spinodal curve on the high-concentration side of the latter, whereas MCT predicts the possibility that for large values of z the glass transition preempts the gas–liquid phase separation.

The specific results of the SCGLE theory are in reality also a consequence of the specific static structural properties of the system under study, since these structural properties are employed as input of the dynamic theory. Thus, here we also turned to the discussion of the structure provided by the mean spherical approximation for the HSAY model. In the process, we also discussed the temperature and volume fraction dependence of the compactness of the short-ranged local structure of the system. Let us stress that the semi-analytic solution of the MSA provided us with a unique opportunity to discuss this issue in the context of the simplest non-trivial model. It is natural to question, however, the physical significance of these results for $g(r)$ inside the spinodal. Our assumption is that they describe the structure

of a thermodynamically unstable homogeneous equilibrium state (just like the van der Waals isotherms inside the spinodal represent the pressure of a homogeneous fluid in those thermodynamically unstable states). These unstable states are of limited interest if we are only interested in describing thermodynamically stable, phase-separated conditions. If, however, the conditions for dynamic arrest occur in this region of unstable equilibrium homogeneous states, one may expect the freezing in time of these locally compact and inhomogeneous (but globally homogeneous) states described by the MSA inside the spinodal line.

In reference to the possible detailed comparison of our findings with concrete experimental measurements, so far not many experimental reports of the determination of the glass transition line for this kind of system have appeared in the literature. As discussed in the previous section, the predictions of the SCGLE theory for a mono-disperse suspension should apply most naturally to the system studied in [14–16], since the origin of the short-ranged attractions is not derived from the presence of a second colloidal component. Unfortunately, the comparison between these measurements and the predictions of the SCGLE theory (complemented with the MSA static structure of the attractive Yukawa model) is not straightforward in the absence of a reliable connection between the experimental control parameters and the theoretical variables K, z, and ϕ.

On the other hand, the most extensive and straightforward determination of the transition line exhibiting reentrance has been performed on the colloid–polymer mixture reported in [18]. As discussed above, neither MCT nor the present theory are capable of providing a really satisfactory fit of the experimentally determined glass transition line. The origin of this discrepancy is perhaps not to be found in an intrinsic failure of these dynamic theories, but in the very fact that the mono-component versions of these theories are meant to apply only to genuine mono-disperse systems; systems with depletion forces in principle do not belong to this category. This amounts to questioning the limits of validity of the (Asakura–Oosawa or any other) representation of these systems as effective mono-component systems. Finding out whether this possibility would lead to a better interpretation of the available experimental data, however, requires us to place this discussion in the framework of the extension of these theories of dynamic arrest to multi-component systems. This in principle is now possible, since the multi-component extension of MCT has been available for many years [47], and the corresponding extension of the SCGLE theory has just been elaborated [48]. Preliminary work [49] indicates that this extension to mixtures of the SCGLE theory indeed seems to provide a remarkably simple physical picture and an unexpectedly accurate fit of the experimental data of the dynamic arrest phase diagram in the colloid polymer mixtures reported by Pham *et al* [18]. An important step in that direction was to first attempt to fit those experimental data with the mono-component SCGLE theory, as originally done with MCT [18], and as we attempted to do as part of the present work. The negative result hints at the possible inadequacy of the application of mono-component theories of dynamic arrest to these intrinsically bi-disperse systems. This leaves genuinely mono-disperse systems as the natural area of application of the results presented here. A more significant comparison with experimental measurements must await, however, the report of more abundant measurements. In the meanwhile, the application of the SCGLE theory to mono-disperse model systems with short-ranged attractions will allow us to address fundamental questions, such as the relationship between dynamic arrest, gas–liquid coexistence, and the gel and glass transitions.

Acknowledgments

This work was supported by the Consejo Nacional de Ciencia y Tecnología (CONACYT, México) through grant No. C01-47611.

References

[1] Angell C A 1995 *Science* **267** 1924
[2] Debenedetti P G and Stillinger F H 2001 *Nature* **410** 359
[3] Götze W 1991 *Liquids, Freezing and Glass Transition* ed J P Hansen, D Levesque and J Zinn-Justin (Amsterdam: North-Holland)
[4] Pusey P N 1991 *Liquids, Freezing and the Glass Transition* ed J P Hansen, D Levesque and J Zinn-Justin (Amsterdam: Elsevier)
[5] Hess W and Klein R 1983 *Adv. Phys.* **32** 173
[6] Nägele G 1996 *Phys. Rep.* **272** 215
[7] Sciortino F and Tartaglia P 2005 *Adv. Phys.* **54** 471
[8] Das S P 2004 *Rev. Mod. Phys.* **76** 785
[9] Götze W and Sjögren L 1992 *Rep. Prog. Phys.* **55** 241
[10] van Megen W and Pusey P N 1991 *Phys. Rev.* A **43** 5429
[11] Bergenholtz J and Fuchs M 1999 *Phys. Rev.* E **59** 5706
[12] Fabbian L, Götze W, Sciortino F, Tartaglia P and Thiery F 1999 *Phys. Rev.* E **59** R1347
[13] Dawson K, Foffi G, Fuchs M, Götze W, Sciortino F, Sperl M, Tartaglia P, Voigtmann Th and Zaccarelli E 2000 *Phys. Rev.* E **63** 011401
[14] Mallamace F, Gambadauro P, Micali N, Tartaglia P, Liao C and Chen S-H 2000 *Phys. Rev. Lett.* **84** 5431
[15] Chen S-H, Chen W-R and Mallamace F 2003 *Science* **300** 619
[16] Chen W-R, Mallamace F, Glinka C J, Fratini E and Chen S-H 2003 *Phys. Rev.* E **68** 041402
[17] Segré P N, Prasad V, Schofield A B and Weitz D A 2001 *Phys. Rev. Lett.* **86** 6042
[18] Pham K N *et al* 2002 *Science* **296** 104
[19] Eckert T and Bartsch E 2002 *Phys. Rev. Lett.* **89** 125701
[20] Poon W C K 2002 *J. Phys.: Condens. Matter* **14** R859
[21] Foffi G, De Michele C, Sciortino F and Tartaglia P 2005 *Phys. Rev. Lett.* **94** 078301
[22] Zaccarelli E, Löwen H, Wessels P P F, Sciortino F, Tartaglia P and Lykos C N 2004 *Phys. Rev. Lett.* **92** 225703
[23] Szamel G 2003 *Phys. Rev. Lett.* **90** 228301
[24] Wu J and Cao J 2005 *Phys. Rev. Lett.* 078301 **95**
[25] Mayer P, Miyazaki K and Reichman D R 2006 *Phys. Rev. Lett.* **97** 095702
[26] Tokuyama M 2000 *Phys. Rev.* E **62** R5915
[27] Ramírez-González P, Juárez-Maldonado R, Yeomans-Reyna L, Chávez-Rojo M A, Chávez-Páez M, Vizcarra-Rendón A and Medina-Noyola M 2007 *Rev. Mex. Fis.* **53** 327 (http://rmf.fciencias.unam.mx/pdf/rmf/53/5/53_5_327.pdf)
[28] Yeomans-Reyna L, Chávez-Rojo M A, Ramírez-González P E, Juárez-Maldonado R, Chávez-Páez M and Medina-Noyola M 2007 *Phys. Rev.* E **76** 041504

[29] Juárez-Maldonado R, Chávez-Rojo M A, Ramírez-González P E, Yeomans-Reyna L and Medina-Noyola M 2007 *Phys. Rev.* E **76** 062502
[30] Yeomans-Reyna L and Medina-Noyola M 2001 *Phys. Rev.* E **64** 066114
[31] Yeomans-Reyna L, Acuña-Campa H, Guevara-Rodríguez F and Medina-Noyola M 2003 *Phys. Rev.* E **67** 021108
[32] Chávez-Rojo M A and Medina-Noyola M 2006 *Physica* A **366** 55
[33] Chávez-Rojo M A and Medina-Noyola M 2005 *Phys. Rev.* E **72** 031107
[34] Nägele G, Bergenholtz J and Dhont J K G 1999 *J. Chem. Phys.* **110** 7037
[35] Cichocki B and Hess W 1987 *Physica* A **141** 475
[36] Medina-Noyola M 1987 *Faraday Discuss. Chem. Soc.* **83** 21
[37] Medina-Noyola M and del Río-Correa J L 1987 *Physica* A **146** 483
[38] Vineyard G H 1958 *Phys. Rev.* **110** 999
[39] Arauz-Lara J L and Medina-Noyola M 1983 *Physica* A **122** 547
[40] Hansen J P and McDonald I R 1976 *Theory of Simple Liquids* (New York: Academic)
[41] Høye J S and Blum L 1977 *J. Stat. Phys.* **16** 399
[42] Hansen J P and Verlet L 1969 *Phys. Rev.* **184** 151
[43] Germain Ph and Amokrane S 2007 *Phys. Rev.* E **76** 031401
[44] Zaccarelli E, Foffi G, Dawson K A, Sciortino F and Tartaglia P 2001 *Phys. Rev.* E **63** 031501
[45] Asakura S and Oosawa F 1954 *J. Chem. Phys.* **22** 1255
[46] Grant M C and Russel W B 1993 *Phys. Rev.* E **47** 2606
[47] Bosse J and Thakur J S 1987 *Phys. Rev. Lett.* **59** 998
[48] Juárez-Maldonado R and Medina-Noyola M 2007 *Phys. Rev.* E at press
(Juárez-Maldonado R and Medina-Noyola M 2007 *Preprint* 0711.2021v1 [cond-mat.mtrl-sci])
[49] Juárez-Maldonado R and Medina-Noyola M 2008 in preparation